Dust particle pair correlation functions and the non-linear effect of interaction potentials

Jie Kong, Ke Qiao, Lorin S. Matthews, and Truell W. Hyde
Center for Astrophysics, Space Physics, and Engineering Research (CASPER), Baylor University, Waco, Texas 76798-7310, USA

Abstract

Dust temperature is a measure of the energy of the stochastic motion of a dust particle, and is a result of the combination of the Brownian motion and the fluctuations in the dust charge and confining electric field. A method using the equilibrium value of the mean square displacement was recently introduced to obtain the dust temperature experimentally. As a follow up, this paper investigates the relationship between the temperature derived from the mean square displacement technique and a technique using the probability distribution of the displacements obtained from random fluctuations of the dust particle. Experimental results indicate that the harmonic confinement potential acting on the dust particle can be obtained by combining the two methods, allowing the non-linear effect of the confining force to be investigated. The thermal expansion in a one-dimensional vertical chain is discussed as a representative application as it is related to the non-linear confinement force, or the asymmetric confinement potential.

1. Introduction

The temperature of a dust particle in dusty plasma is a combination of Brownian motion and fluctuations of the electric field and dust charge [1 – 9]. Experimentally, the dust temperature can be derived from the Gaussian velocity distribution, where the dust velocity is usually calculated from the position difference between subsequent frames of high speed video of the particle motion. Recently, we introduced a dust temperature measurement technique based on the mean square displacement (MSD) method [10 – 14]. Important information, such as the dust particle resonance frequency, neutral drag coefficient and dust temperature, can be easily extracted from the MSD experimental data. Since the MSD calculation uses only the displacement of the particles from the initial image frame, the cumulative errors inherent to other methods generated from the calculation of velocity can be reduced. Another benefit is that using the equilibrium value of the MSD to calculate the dust temperature significantly reduces the influence of un-wanted continuous coherent oscillations in the system confinement [10].

The position fluctuation of a single dust particle confined in a harmonic potential can be described by the Langevin equation, which for one-dimensional motion [11] is given by $m\ddot{x} \rightarrow m\gamma v - m\omega_0^2 + R(t)$ (1)

where m is the mass, γ is the Epstein friction coefficient [15], ω_0 is the resonance frequency, and $R(t)$ is a random force. The MSD solution to Eq 1 is $\left\langle x^2 \right\rangle = A_0\left[1-\exp\left(-\frac{\gamma\tau}{2}\right)\left\{\cos\left(\hat{\omega}\tau\right)-\frac{\gamma}{2\hat{\omega}}\sin\left(\hat{\omega}\tau\right)\right\}\right]$ (2)

where $A_0 = \frac{2k_BT}{m\omega_0^2}$ is the equilibrium value as $\tau \to \infty$, and $\hat{\omega} = \sqrt{\omega_0^2 - \left(\frac{\gamma}{2}\right)^2}$. Experimental data for a particle's position fluctuation can be used to generate the MSD as a function of the elapsed time. A fit to this data using

Eq 2 then allows determination of the experimental parameters such as dust temperature T, the Epstein drag coefficient γ, and the resonance frequency ω_0. Since this technique is based solely on the fluctuating dust positions, it has the added benefit of requiring no external perturbation to the dusty plasma environment.

For a two-particle system, the correlated Langevin equations can be separated into two independent Langevin equations by using of the center of mass (CM) coordinates and positions relative to the CM of the system. In this case, the equation of motion for the CM and relative coordinates exhibit a simple form similar to Eq 1. In this case, the Langevin equation of motion for the relative coordinates also reflects the interaction between the two particles, which contributes to the overall confinement potential.

It is well known that approximating the confinement potential of an individual particle as a quadratic function of the displacement from equilibrium is generally adequate for small fluctuations or low dust temperature. However, for higher dust temperatures, or a confinement potential having significant asymmetry, non-linear effects can no longer be ignored. Additional terms of the form $B_2x^2 + B_3x^3 + \ldots$, where B_i, $i = 2, 3, \ldots$ are constants, must to be added to Eq. 1 to model these forces more accurately. Obtaining a mathematical solution to the non-linear equation that arises for a particle under forced oscillation is complicated [16, 17]. To obtain an analytical solution of the non-linear Langevin equation with a random force term $R(t)$ (as in Eq 1) is much more difficult.

Experiments which allow one to obtain information about the non-linear response of dust particles, especially the non-linear interactions that can arise between dust particles, can yield deeper insight to the understanding of the dusty plasma properties. Asymmetric interaction forces acting on the dust particles, such as the ion drag force or the ion-focusing effect in the vertical direction [18, 19], are an area of increasing research interest [20].

In this paper we present a technique for investigating the local confinement potential based on the distribution of dust particle position fluctuations and the MSD method. Section 2 provides the theoretical background for using the probability distribution function (PDF) of the particle positions to calculate the confining potential. Section 3 presents the results of applying these two methods to experimental data. A comparison of the position probability distribution and MSD techniques is presented in Section 4, and the feasibility of using these techniques to derive non-linear coefficients of the interaction force is discussed. Section 5 presents an application of using the obtained non-linear coefficient to study the one-dimensional thermal expansion coefficient. Conclusions are presented in Section 6.

2. Theoretical background

A two-particle correlation density distribution function $f(\vec{r}_1 - \vec{r}_2)$ represents a joint probability for the relative position between the two particles, with the corresponding pair correlation function defined as [21]

$$g_2(\vec{r}) = \left\langle \left[r_{x1} - r_{x2}, r_{y1} - r_{y2}, z_1 - z_2 \right] \right\rangle \qquad (3)$$

For a two-particle system, the particle pair has cylindrical symmetry. Anticipating our experimental conditions, we take, $r_i = r_{xi}$, to represent the displacement from the horizontal direction (perpendicular to gravity) and $h_i = z_i$ to represent the position of each particle along the vertical direction (parallel to gravity). This allows Eq 3 to be rewritten as, $g_2(r,h) = \left\langle f\left(\left[r_1 - r_2, h_1 - h_2\right], t\right)\right\rangle = \left\langle f\left(\left[r,h\right], t\right)\right\rangle$ (4)

where $r = r_1 - r_2$, $h = h_1 - h_2$. Notice that this form of Eqs 3 and 4 can also be used for the CM case (or sloshing mode) simply by making the replacement $r = \dfrac{m_1 r_1 + m_2 r_2}{m_1 + m_2}$ and $h = \dfrac{m_1 h_1 + m_2 h_2}{m_1 + m_2}$. Since the forces acting on the

particle pairs are derived from potentials, the probability of finding a particle at any particular location is related to the potential energy distribution at that location. This can be described by Boltzmann's equation [22 – 28],

$$g_2(r,h) = a_0 \exp\left(-\frac{\varphi(r,h)}{k_B T}\right) = a_0 \exp\left(-\psi(r,h)\right) \qquad (5)$$

where a_0 is a constant, $\varphi(r,h)$ is the confining potential energy, $k_B T$ is the particle temperature and $\psi(r,h) = \varphi(r,h)/k_B T$ is the dimensionless potential.

For small displacements about the equilibrium position $x = [r,h]$, $\varphi(x)$ can be expanded as

$$\begin{aligned}&\varphi(x)\\ &= \varphi_0 + \frac{\varphi'}{1!}(x-x_0) + \frac{\varphi''}{2!}(x-x_0)^2 + \frac{\varphi'''}{3!}(x-x_0)^3 + \ldots \qquad (6)\\ &= p_{\varphi 0} + p_{\varphi 1}(x-x_0) + p_{\varphi 2}(x-x_0)^2 + p_{\varphi 3}(x-x_0)^3 + \ldots\end{aligned}$$

where primes denote the derivative with respect to x, and $p_{\varphi i}$ represents the i^{th} coefficient of the polynomials. A convenient potential zero can be chosen such that $p_{\varphi 0} = 0$ and $p_{\varphi 1} = 0$. Thus for small displacements, the restoring force can be linearized and the potential $\varphi(x) = p_{\varphi 2} x^2$ is quadratic in the displacement x, with coefficient $p_{\varphi 2} = \frac{1}{2} m\omega_0^2$, where ω_0 is the particle's resonance frequency. In the following, we will focus on the vertical direction h, i.e., $x = h$. Substituting Eq 6 into Eq 5 yields

$$\begin{aligned}\psi(h) &= \psi_0 - \ln\left(g_2(h)\right)\\ &= P_0 + P_1\Delta h + P_2\Delta h^2 + P_3\Delta h^3 + \ldots\end{aligned} \qquad (7)$$

where $P_i = p_{\varphi i}/k_B T$ and P_0 and P_1 are zero by the argument given above. Thus, for a linear restoring force, only P_2 contributes and $\psi(h) = \frac{\varphi(h)}{k_B T} = P_2 \Delta h^2$ (8)

The coefficient P_2 may be determined experimentally by fitting the probability distribution function (PDF) of a particle's position with a Boltzmann distribution, as in Eq 5. When the resonance frequency ω_0 is determined employing some other experimental method, for example the MSD method, the particle temperature can then be derived using Eq 8 and the experimentally determined coefficient P_2.

As noted above, the dust temperature $k_B T$ can also be derived by fitting the MSD calculated for a particle's fluctuating position with an equation of the form shown in Eq 2 to determine the equilibrium value A_0. The relationship between the value of A_0 derived from the MSD and the coefficient P_2 derived from the PDF is given by, $A_0 = \frac{1}{P_2} = \frac{2k_B T}{m\omega_0^2}$ (9)

which can then be employed to serve as a criterion for the validation of the experimental measurement of each value.

Combining the temperature derived from A_0 as obtained from the MSD method and the coefficient P_2 obtained from the PDF of the particle position, the confinement potential $\varphi(h)$ can then be obtained from Eq 8.

This method may be extended to investigate the non-linear effect of the dust particle confinement force by including the higher-order terms shown in equation Eq 7, which is now written as

$$\psi(h) = \frac{m\omega_0^2}{2k_B T}\Delta h^2 + P_3\Delta h^3 + P_4\Delta h^4 + \ldots \qquad (10)$$

The coefficients of the higher-order terms may be determined by fitting the dimensionless potential $\psi(h)$, calculated from the pair correlation function obtained from the experimental data (Eq 7) with a cubic or higher order equation.

3. Experimental application

The experiment described here was performed in a modified gaseous electronics conference (GEC) radio-frequency (RF) cell [29], filled with argon gas at a pressure of 13.3 Pa. An RF electrical field was produced by a pair of capacitively-coupled electrodes 8 cm in diameter, situated one above the other, and separated by a distance of 2.54 cm. The upper electrode was grounded, while the lower electrode was powered by a RF generator at a constant frequency of 13.56 MHz. The amplitude of the input RF signal ranged from 1.5 – 9.0 W. An open- ended glass box of dimension 10.5 mm × 10.5 mm × 12.5 mm (width × depth × height) with 2 mm wall thickness was placed at the center of the lower electrode. Melamine formaldehyde spheres having a manufacturer-specified mass density of 1.51 g/cm^3 and diameter of 8.89 μm were used. A dust dropper was employed to introduce the particles into the glass box, where they were illuminated by a vertical sheet of laser light. The particles' positions were recorded at 500 frames per second (fps) using a side-mounted, high-speed CCD (Photron) camera and a microscope lens. Fig 1 shows sample raw data of the fluctuations of the particle positions.

Because of the statistical nature of the correlation function, the sampling time for the experimental data must be long enough ($t_{Sampling} \to \infty$) to ensure the accuracy of the results. Accordingly, our experimental data were collected using a high-speed camera at 500 fps for a total duration of at least 3 minutes for each experimental run.

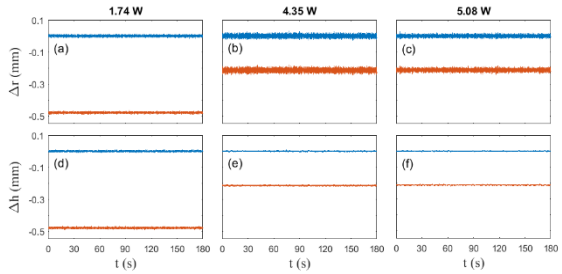

Fig 1. Fluctuations in the (a) – (c) horizontal and (d) – (f) vertical directions for a two-particle vertical chain with RF power 1.74 W, 4.35 W and 5.08 W respectively. The separations between the upper and lower particles shown in the figure are all vertical distances (both particles are at the same mean horizontal positions under all the power settings). The mean vertical separations are 480, 215 and 213 (μm) for RF power 1.74 W, 4.35 W and 5.08 W respectively.

Employing the particle position fluctuation data shown in Fig.1, the density distribution function and pair correlation function $g_2(h_1 - h_2)$ derived from data collected at 1.74 W, 4.35 W and 5.08 W are shown in Fig 2.

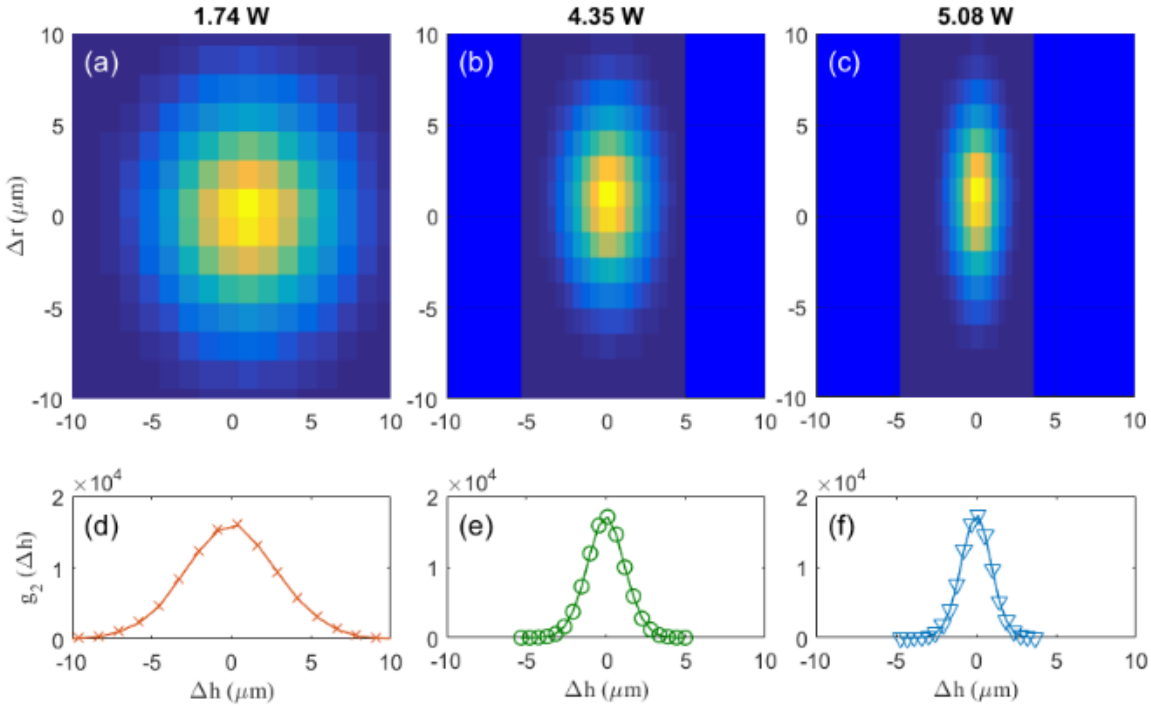

Fig 2. Comparison of experimental results for the distribution function $f_2(r_1 - r_2, h_1 - h_2)$ collected at RF powers of (a) 1.74 W, (b) 4.35 W and (c) 5.08 W, and the corresponding pair correlation function $g_2(\Delta h)$ at (d) – (f).

The dimensionless potential $\psi(\Delta h)$ is calculated from $g_2(\Delta h)$ using Eq 7 with the resulting distribution fit employing a quadratic function as shown in Eq 8. The results for various power settings are shown in Fig 3.

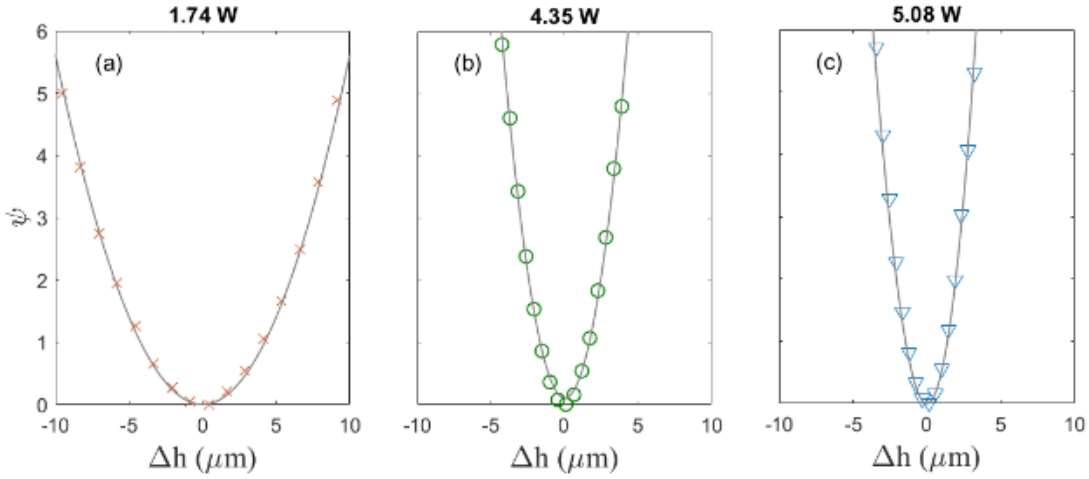

Fig 3. (a) – (c) Experimental dimensionless interaction potentials $\psi(\Delta h)$ (symbols) at RF powers of 1.74 W, 4.35 W and 5.08 W. Quadratic fits are indicated by solid lines. Each $\psi(\Delta h)$ is calculated from the corresponding g_2 shown in Fig 2 (d) – (f).

The particle position data obtained from the experiment were also used to calculate the MSD as shown in Fig 4 for various RF powers. The equilibrium value A_0 and the resonance frequency ω_0 were then derived from the theoretical fit obtained using Eq 2.

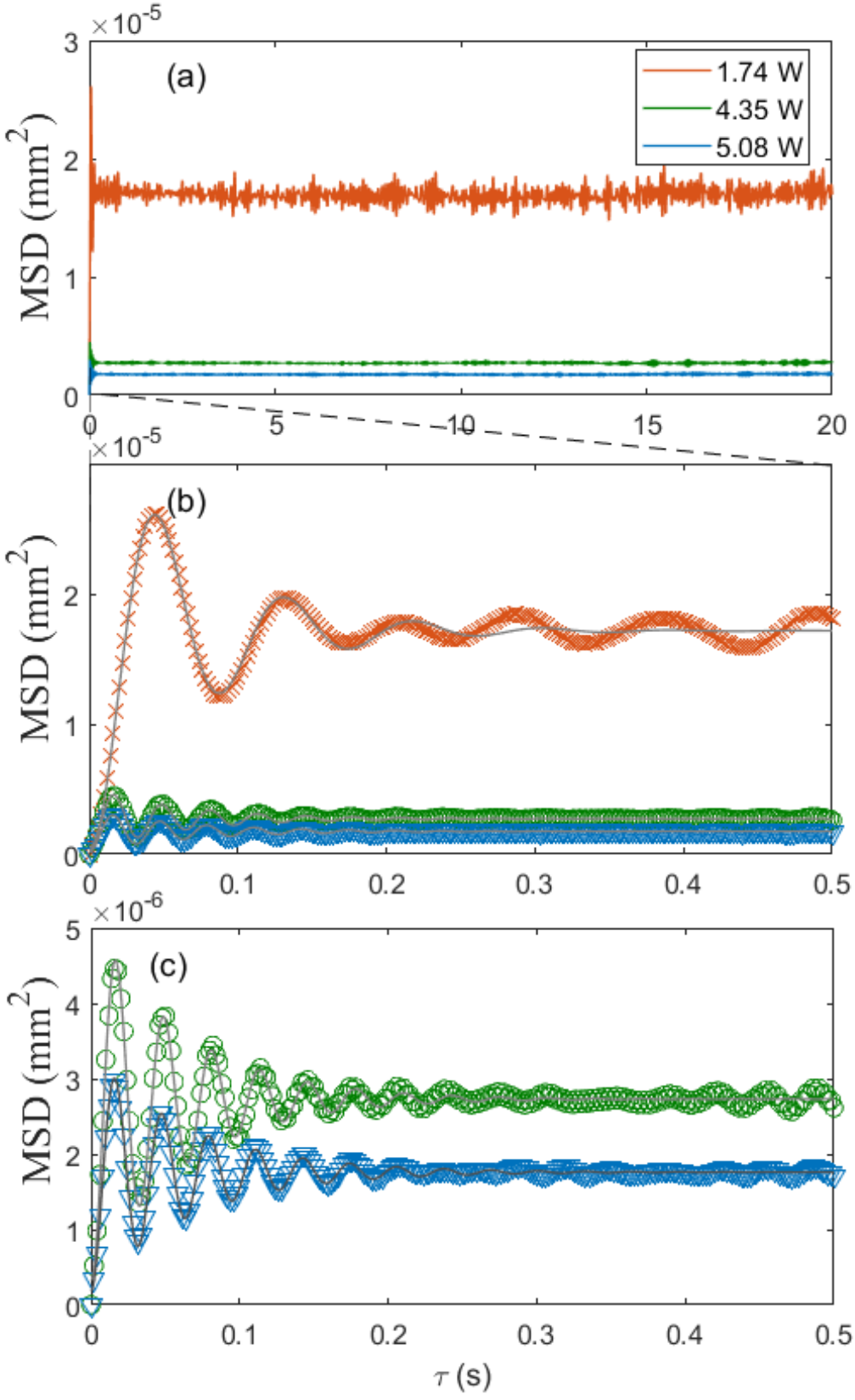
(a)
1.74 W
4.35 W
5.08 W
MSD (mm^2)
$\times 10^{-5}$
(b)
MSD (mm^2)
$\times 10^{-5}$
(c)
MSD (mm^2)
$\times 10^{-6}$
τ (s)

Fig 4. (a) MSD's at RF power settings of 1.74 W, 4.35 W and 5.08 W. (b) Corresponding expanded view of (a) for $\tau \leq 0.5\,\mathrm{s}$ (symbols) and corresponding theoretical fits (solid lines) obtained using Eq 2. (c) Details for 4.35 W and 5.08 W from (b).

As indicated in Fig 4, the equilibrium value A_0 increases as the RF power decreases. It can also clearly be seen that the oscillation frequency increases as the RF power increases. These data are shown over a range of RF powers from 1.5 – 7.4 W in Fig 5a, b. The experimentally derived equilibrium value of the MSD, A_0, and the inverse of the quadratic coefficient P_2, obtained from the dimensionless potential ψ are compared in Fig 5a. As shown, the values are almost identical across the RF power range. Thus, the two methods yield consistent results, as required by the relationship given in Eq 9.

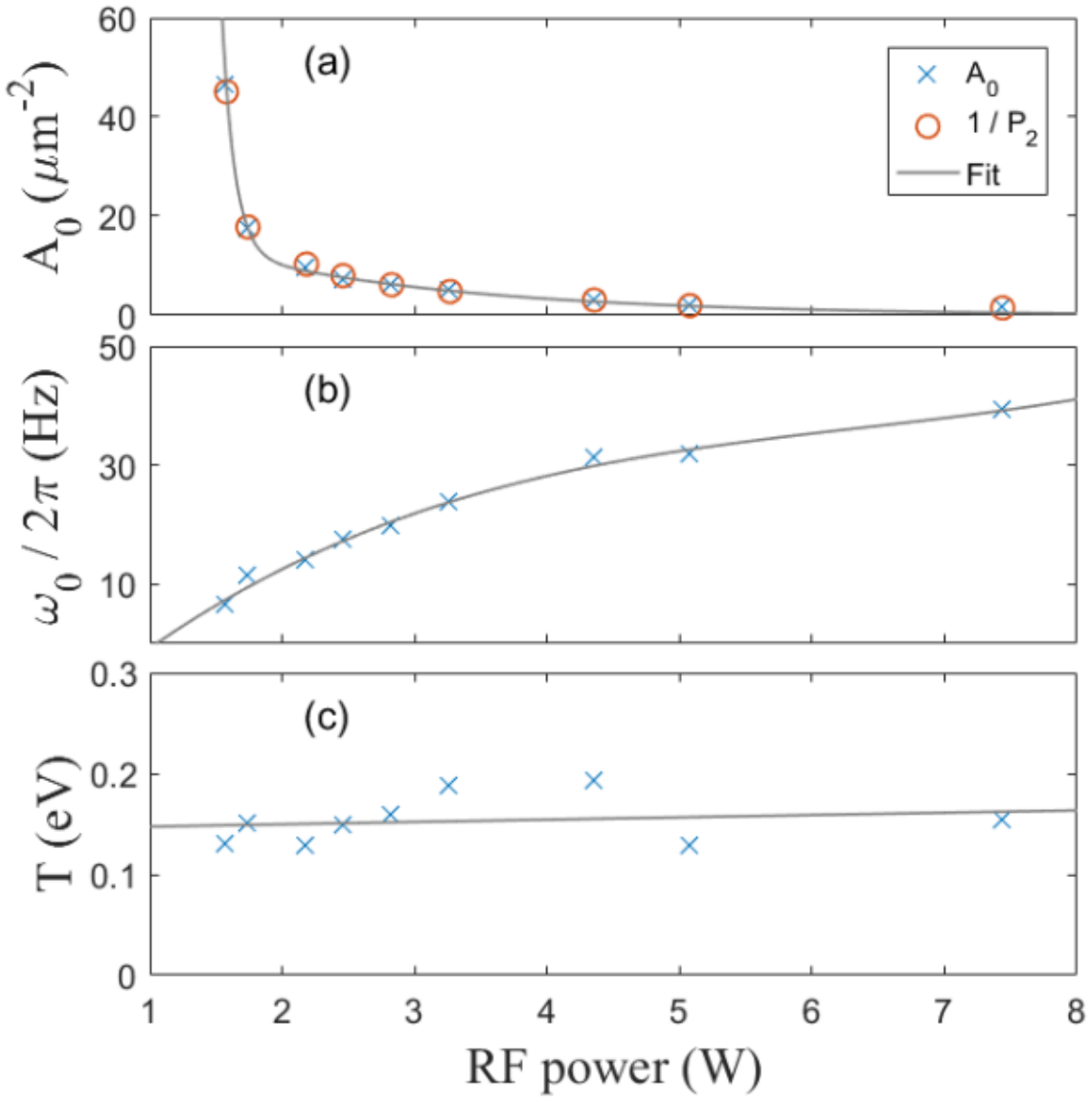

Fig 5. (a) Comparison of A_0 and $1/P_2$ as a function of RF power. (b) Resonance frequency $\omega_0/2\pi$ derived from MSD method illustrated in Fig 4. (c) Dust temperature calculated from $k_BT = A_0 m\omega_0^2/2$ using the values from (a) and (b). The trend lines are shown to guide the eyes.

The dust temperature can also be obtained from the MSD technique (Fig 5c), allowing the potential $\varphi(h) = (k_BT)\psi(h)$ to be calculated. In the following analysis, φ_2 and φ_3 are used to represent quadratic and cubic polynomials, respectively, for the potential fits.

4. Analysis and discussion

As shown in Fig 5a, the experimental values for the equilibrium value A_0 of the MSD and the inverse of the quadratic parameter P_2 of the dimensionless potential ψ are almost identical, as predicted by Eq 9. It is important to note that the two techniques use entirely different statistical methods: the MSD technique is focused on the temporal correlations while the PDF method of using g_2 is determined by the fluctuations shown in the distribution of the spatial separations between the two particles. Thus, the experimental results shown in Fig 5a confirm that the dust temperature derived from the MSD method represent the stochastic motions of the dust particle and are valid for use in the Boltzmann distribution (Eq 5) to determine the potential.

The advantages of using the MSD technique over other methods to derive the dust temperature are discussed in detail in reference [10]. Additionally, the temporal distribution obtained from the MSD technique is self-sufficient, i.e., the dust temperature can be directly calculated from the measured values of A_0 and ω_0, while the spatial (Boltzmann) distribution measured from the PDF of the particle positions must rely on other techniques to provide a separate measurement of the oscillation frequency ω_0 so that the dust temperature T can be calculated from P_2. However, there is one important advantage of using the spatial distribution g_2, the investigation of the non-linearity of the interaction force.

As mentioned in Section 1, to include non-linear effects, the Langevin equation must be modified to include higher-order terms, $m\ddot{x} = -m\gamma\dot{x} - m\omega_0^2 x + R(t) + B_2x^2 + B_3x^3 + \ldots$ (11)

It is difficult to solve Eq 11 mathematically. Additionally, for random fluctuations of small amplitude, it is questionable whether the deviations in the MSD result caused by any such non-linear effects can be resolved experimentally. On the other hand, assuming a Boltzmann distribution representation for g_2 and fitting the dimensionless potential ψ employing a higher order polynomial, as expressed by Eqs 6 and 7, is simple, as shown in the example below.

In the following discussion, sine the fluctuation amplitude is small, only the cubic term is included in the analysis. Therefore, the quadratic term remains the dominant term.

The non-linear coefficients P_3 and $p_{\varphi 3}$ are derived from fitting the potential distributions $\psi(h)$ and $\varphi(h)$, respectively. P_3 is derived by fitting the potential distribution $\psi(h)$ obtained from the spatial correlation g_2, and $\varphi(h) = (k_BT)\cdot\psi(h)$, which also requires a value of the temperature measured using the MSD method, is shown in Fig 6 (a) and (b) as a function of RF power. The potential is also shown as a function of the vertical particle separation in Fig 6c.

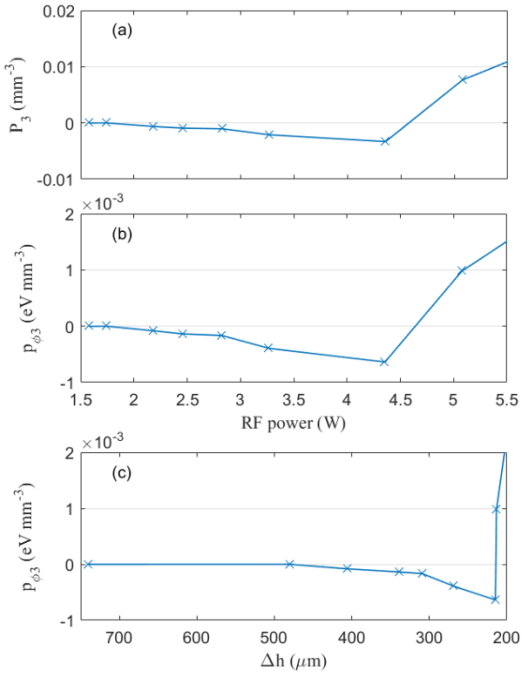

Fig 6. (a) Cubic coefficient $p_{\varphi 3}$ of the dimensionless potential ψ_3 as a function of the applied RF power. (b) $p_{\varphi 3}$ of the confinement potential φ_3 as a function of the applied RF power, and (c) $p_{\varphi 3}$ as a function of the separation between the two particles.

As can be seen in Fig 6c, for large separation, i.e., $h > 400\ \mu m$, $p_{\varphi 3}$ is close to zero, implying that the potential is parabolic. For separations between $214 < h < 400\ \mu m$, $p_{\varphi 3}$ is negatively increasing in magnitude as the separation decreases. It is important to note that rapid sign change from negative to positive occurs as the particle separation decreases to $h \sim 214 \mu m$. Since the cubic parameter $p_{\varphi 3}$ represents the asymmetric shape of the confinement potential, its sign determines the 'softer side' of the potential. The implications of this will be discussed in the following section.

5. One-dimensional thermal expansion coefficient

One of the applications of the non-linear confinement force is to study the linear thermal expansion of a crystal structure. The linear thermal expansion of a one-dimensional crystal structure ΔL as a function of the temperature change ΔT is given by [30]

$$\Delta L = \alpha_L L_0 \Delta T \qquad (12)$$

where α_L is the linear thermal expansion coefficient, and L_0 is the original length of the crystal. Figure 9 shows the thermal expansion in a Lennard-Jones potential [31].

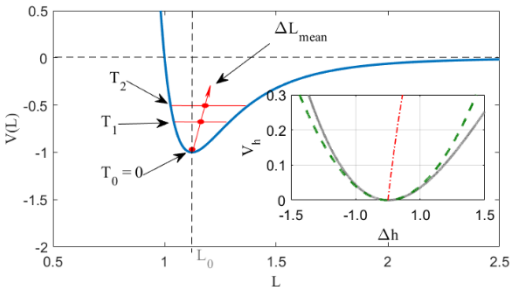

Fig 7. The mean displacement ΔL_{mean} (relative to the zero-temperature equilibrium position L_0) in a Lennard-Jones potential. The asymmetric potential, with the 'softer side' of the potential for $L > L_0$, causes the mean displacement to increase as the confined particle temperature increases. Similarly, the inset shows a parabolic potential (dashed) with a cubic function potential (solid) with the non-zero mean displacement indicated (dash-dot).

As shown in Fig 7, a particle will be confined at the potential minimum located at L_0 when its temperature is $T_0 = 0$. As the particle temperature increases, the mean displacement will increase to $\bar{L} = L_0 + \Delta L_{mean}$, indicating a positive coefficient of thermal expansion. For small displacements (low particle temperature), the asymmetric potential can be described by a cubic polynomial. The sign of the cubic parameter determines the direction of the softer side. As shown in the inset, a cubic potential with a negative $p_{\varphi 3}$ has a softer side for $\Delta h > 0$, as is seen in a Lennard-Jones potential. The softer side will move to $\Delta h < 0$ if the cubic parameter is positive. This will cause the mean displacement to decrease as temperature increases, which is the origin of negative thermal expansion [32 – 36]. Therefore, the cubic parameter $p_{\varphi 3}$ can be used to study the linear thermal expansion. Cubic fits to the experimentally measured potentials are shown in Fig 8 for two different particle separations on either side of the critical value of $\Delta h = 214\ \mu m$ shown in Fig 6c. At RF power 4.35 W, the particle separation is 215 μm, and $p_{\varphi 3}$ is negative, while the slightly smaller particle separation of 2.13 μm at 5.08 W yields a positive value of $p_{\varphi 3}$.

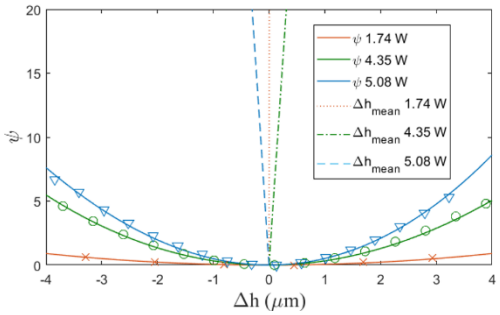

Fig 8. The mean displacement relative to the equilibrium point at different particle energy levels (kinetic temperature), calculated using the cubic potential obtained from experimental data (symbols). Solid lines are cubic fits of the potential for equilibrium separations of 480 μm (RF power 1.74 W), 215 μm (RF power 4.35 W) and 2.13 μm (RF power 5.08 W). The mean displacement at RF power 1.74 W, where the cubic coefficient is determined to be near zero, is almost expansion-less.

As shown in Fig 8, the mean displacement Δh_{mean} is zero for a parabolic potential ($p_{\varphi 3} \sim 0$) at RF power 1.74 W (dotted line). As the RF power is increased to 4.35 W, the particle separation decreases to 215 μm, and the

cubic parameter changes to a negative value. The corresponding mean displacement Δh_{mean} increases positively as the particle energy level increases, indicative of a positive thermal expansion. As the RF power is further increased to 5.08 W, the cubic parameter $p_{\varphi 3}$ changes to a positive value. The corresponding mean displacement Δh_{mean} increases negatively as the particle energy level increases, which is a negative thermal expansion. This sign change is most likely related to the ion focusing effect [18, 19]. Changing the system RF power has an effect on the ion Mach number, moving the ion focusing region. It is speculated that the ion focusing region may change from a location between the two particles to a location which is down stream of both particles. This is a subject of further investigation.

6. Conclusions

A comparison of experimentally determined temperatures and confinement potentials for an interacting pair of dust grains immersed in a complex plasma environment has been made using two different methods. The mean square displacement (MSD) method takes advantage of *temporal* correlations in the particles' positions to determine the particles' resonance frequency ω_0 from the evanescent oscillation (c.f. Fig 4).

On the other hand, the probability distribution function (PDF) takes advantage of the *spatial* variations in the particles' positions. The experimental results shown in Fig 5a confirm the theoretical equivalence of these two techniques. Therefore, either the MSD or the PDF method can be used to examine the dust temperature, although the PDF method requires the resonance frequency to be measured separately using a different technique.

It is important to note that use of the PDF method offers the advantage that the potential derived experimentally is the *actual* local confinement potential, making no *a priori* assumptions about its form. Given small fluctuation amplitudes, the simplifying assumption that the confining force is linear may be made, allowing the potential to be treated as quadratic. The nonlinear effects of the confinement force can be investigated by including the contribution of an additional cubic term in the potential. The result shows that at large separation distances the nonlinear coefficient is almost zero. As the separation distance decreases the nonlinear coefficient becomes negative. Interestingly, a transition occurred at $h \sim 214 \mu m$ where the nonlinear coefficient rapidly changes sign from negative to positive as the particle pair separation decreases. The asymmetric confinement potential is related to the structural linear thermal expansion when the cubic parameter of the confinement potential is not zero. When the sign of the cubic parameter of the asymmetric confinement potential is negative, the linear thermal expansion is normal, i.e., the structure dimension increases as the temperature increases. Our experimental result shows that a negative linear thermal expansion occurred as $h < 214\ \mu m$. The cause of this change is currently unclear and will be the subject of continued investigation.

7. Acknowledgments

The authors gratefully acknowledge support from NSF grants No. 1740203, 1414523 and NASA JPL control No. 151701.

References

1. G. E. Morfill and H. Thomas, *Plasma crystal*, J. Vac. Sci. Technol. A14, 490 – 490, (1996).
2. V. V. Zhakhovski , V. I. Molotkov, A. P. Nefedov, V. M. Torchinski , A. G. Khrapak, and V. E. Fortov, *Anomalous heating of a system of dust particles in a gas-discharge plasma*, JETP Lett. 66, 419 – 425, (1997).
3. R. A. Quinn and John Goree, *Experimental investigation of particle heating in a strongly coupled dusty plasma*, Phys. Plasmas 7, 3904-3911, (2000).
4. R. A. Quinn and John Goree, *Single-particle Langevin model of particle temperature in dusty plasmas,* Phys. Rev. E61, 3033-3041, (2000).
5. O. S. Vaulina, S. A. Khrapak, A. P. Nefedov, and O. F. Petrov, *Charge fluctuation-induced heating of dust particles in a plasma*, Phys. Rev. E60, 5959 – 5964, (1999).
6. O. S. Vaulina, *Transport properties of non-ideal systems with isotropic pair interactions between particles*, Plasma Phys. Rep. 30, 652 – 661, (2004).
7. O. S. Vaulina, S. V. Vladimirov, A. Yu. Repin, J. Goree, *Effects of electrostatic plasma oscillations on the kinetic energy of a charged macroparticle*, Phys. Plasmas, 13, 012111, (2006).
8. U. Seifert, *Stochastic thermodynamics, fluctuation theorems and molecular machines*, Rep. Prog. Phys., 75, 126001, (2012).
9. Yan Feng, J. Goree, and Bin Liu, *Errors in particle tracking velocimetry with high speed camera*, Rev. Sci. Instrum. 82, 053707, (2011).
10. J. Kong, K. Qiao, L. S. Matthews and T. W. Hyde, *Temperature measurement of a dust particle in a RF plasma GEC reference cell*, J. Plasma Phys. 82, 905820505, (2016).
11. P. Langevin, *Sur la the´orie du mouvement brownien*, C. R. Acad. Sci. (Paris) 146, 530 – 533, (1908).
12. R. Kubo, *The fluctuation-dissipation theorem*, Rep. Prog. Phys., 29, 255 – 284, (1968).
13. T. Li and M. G. Raizen, *Brownian motion at short time scales*, Ann. Physik, 525, 281 – 295, (2013).
14. T. Li, S. Kheifets, D. Medellin, and M. G. Raizen, *Measurement of the instantaneous velocity of a Brownian particle*, Science, 328, 1673 – 1675, (2010).
15. P. Epstein, *On the resistance experienced by spheres in their motion through gases*, Phys. Rev., 23, 710 – 733, (1924).
16. H. G. Kadji, B. R. Nana Nbendjo, J. B. Chabi Orou, and P. K. Talla, *Nonlinear dynamics of plasma oscillations modeled by a harmonic oscillator*, Phys. Plasmas, 15, 032308 (2008).
17. A. F. El-Bassiouny and M. Eissa, *Dynamics of a single-degree-of-freedom structure with quadratic, cubic and quartic non-linearities to a harmonic resonance*, Appl. Math. Comput., 139, 1 – 21, (2003).
18. M. Lampe, R. Goswami, Z. Sternovsky, S. Robertson, V. Gavrishchaka, G. Ganguli and G. Joyce, *Trapped ion effect on shielding, current flow, and charging of a small object in a plasma*, Phys. Plasmas, 10, 1500 – 1513, (2003).
19. M. Lampe, V. Gavrishchaka, G. Ganguli, and G. Joyce, *Effect of trapped ions on shielding of a charged spherical object in a plasma*, Phys. Rev. Lett., 86, 5278 – 5281, (2001).
20. W. J. Miloch, *Simulations of several finite-sized objects in plasma*, Procedia Comp. Sci., 51, 1282 – 1291, (2015).
21. G. E. Astrakharchik, G. D. Chiara, G. Morigi, and J. Boronat, *Thermal and quantum fluctuations in chains of ultracold polar molecules*, J. Phys. B At. Mol. Opt. Phys., 42, 154026, (2009).
22. D. C. Prieve, *Measurement of colloidal forces with TIRM*, Adv. Colloid Interface Sci., 82, 93, (1999).
23. M. A. Brown, A. L. Smith, and E. J. Staples, *A method using total internal reflection microscopy and radiation pressure to study weak interaction forces of particles near surfaces*, Langmuir, 5, 1319 – 1324, (1989).
24. M. A. Brown and E. J. Staples, *Measurement of absolute particle-surface separation using total internal reflection microscopy and radiation pressure forces*, Langmuir, 6, 1260 – 1265, (1990).
25. V. Blickle, T. Speck, L. Helden, U. Seifert, and C. Bechinger, *Thermodynamics of a colloidal particle in a time dependent non-harmonic potential*, Phys. Rev. Lett., 96, 070603, (2006).
26. N. A. Frej and D. C. Prieve, *Hindered diffusion of a single sphere very near a wall in a nonuniform force field*, J. Chem. Phys., 98, 7552 – 7564, (1993).
27. M. A. Bevan and D. C. Prieve, *Hindered diffusion of colloidal particles very near to a wall: Revised*, J. Chem. Phys., 113, 1228 – 1236, (2000).

28. S. Chandrasekhar, *Stochastic problems in pphysics and astronomy*, Rev. Mod. Phys., 15, 1 – 89, (1943).
29. J. Kong, T. W. Hyde, L. Matthews, K. Qiao, Z. Zhang, and A. Douglass, *One dimensional vertical dust string in a glass box*, Phys. Rev. E 84, 016411, (2011).
30. P. A. Tipler and G. Mosca, Physics for scientists and engineers, Vol. 1, W. H. Freeman Company, New York 2007.
31. J. E. Lennard-Jones, *On the determination of molecular fields*, Proc. R. Soc. Lond. A, 106 (738), 463 – 477, (1924).
32. K. Rottger, A. Endriss, J. Ihringer, S. Doyle and W. F. Kuhs, *Lattice constants and thermal expansion of H_2O and D_2O Ice Ih between 10 and 265 K*, Acta Crystallogr., B 50, 644–648 (1994).
33. M. C. Rechtsman, F. H. Stillinger, and S. Torquato, *Negative Thermal Expansion in Single-Component Systems with Isotropic Interactions*, J. Phys. Chem. A 111, 12816-12821, (2007).
34. V. A. Kuzkin, *Comment on "Negative Thermal Expansion in Single-Component Systems with Isotropic Interactions"*, J. Phys. Chem. A 118, 9793-9794, (2014).
35. Z. Liu, Y. Wang and S. Shang, Origin of negative thermal expansion phenomenon in solids, scripta Materialia, 65, 664-667, (2011).
36. Z. Liu, Y. Wang and S. Shang, *Thermal Expansion Anomaly Regulated by Entropy*, Scientific Reports, 4, 07043, (2014)
37.